Experimental and numerical impact behavior of fully carbon fiber sandwiches for different core types

ilyas BOZKURT

Muş Alparslan Üniversitesi: Mus Alparslan Universitesi

Mete Onur KAMAN

mkaman@firat.edu.tr

Firat University   https://orcid.org/0000-0003-0178-6079

Mustafa ALBAYRAK

Inonu Universitesi

Research Article

Abstract

The aim of this study is to experimentally and numerically examine the impact strength and damage mechanisms of sandwich composites consisting entirely of fiber reinforced composites for different core geometries. For this purpose, firstly, composite sandwich plates with egg box, lattice and square plate core structures were produced. Low-velocity impact tests were carried out by dropping impactors with hemispherical geometry onto the resulting sandwich structure with three different core geometries, and the effect of the core shape on impact strength was determined. For comparison, the cell width and height of these three different types of core were chosen to be similar. In addition, progressive damage analysis with the finite element method was applied. For this purpose, the MAT-162 material model, which provides three-dimensional progressive damage analysis in composite materials and applies the Hashin Damage Criterion, was preferred to be used in the LS-DYNA® program. When specific loads are compared using a square core specimen under the same conditions, it can be said that the contact force of the egg box structure is higher. While the striker rebounded from the square core at the same impact energy, it pierced the sandwich structure in the egg box and completely damaged the lattice core structure.

1. INTRODUCTION

Sandwich composite structures are widely used in aerospace, sports and automotive applications due to their high stiffness/weight ratio, high strength/weight ratio and energy absorption capacity [1−2]. Sandwich materials are generally formed by combining the core, top cover and bottom cover materials. In general, a sandwich structure consists of thin but rigid face sheets connected to a lightweight core such as a honeycomb, prismatic or lattice core [2−3]. To improve the performance of sandwich structures, new sandwich structures with various face sheet and core material combinations are being developed. Various studies have been conducted using different core structure geometries and materials to increase the high strength/weight ratio of sandwich structures to higher levels [4−12]. Wu et al. [13] investigated the performance of pyramidal lattice cores produced by hot press molding technique and interlocking method under compression and impact. Fracture mechanisms and energy absorption capacity of aluminum sandwich structures were investigated by Hou [14] and Boonkong [15] under impact load and the influencing factors were discussed. Radford et al. [16] investigated the impact behavior of corrugated, pyramidal and aluminum foam core sandwich structures subjected to impact loads. Zhang et al. [17] investigated the quasi-static compression test and weight drop test performance by producing pyramidal lattice core sandwich structures consisting of carbon fiber reinforced polymer (CFRP) surface layers and aluminum alloy cores. Crupi et al. [18] investigated the impact resistance of sandwich structures with glass fiber reinforced composite cover and aluminum foam core. They developed an analytical model to predict the maximum reaction forces under low-velocity impact. Balaban et al. [19] examined the impact behavior of sandwich composite structures with E-glass fiber reinforced polymer material as the upper and lower cover material and PVC foam as the core material. Jiang et al. [20] designed orthogonal sandwich composite panels reinforced with carbon fibers to create sandwich structures with very low specific gravity and applied compression tests. At the end of the test, they examined the specific energy

absorption level and presented the results graphically. Xue et al. [21] developed a carbon/glass fiber hybrid composite sandwich cover with high ductility and strength to increase the impact resistance of the honeycomb sandwich structure under low velocity and heavy load. They examined the effect of thickness and cell size changes of the honeycomb sandwich structure using the finite element method. George et al. [22] manufactured pyramid-shaped cage sandwich cores with relative densities in the range of 1−10% using an interlocking method. Afterwards, the effect of shear force on these sandwich cores was examined numerically and experimentally. Many researchers have focused on compression [18−23] and impact [5, 7, 15, 19, 24−29, 30−36] strength of sandwich plates. In the sandwiches in the studies, as the core structure; Mechanical properties of sandwich plates using honeycomb structure [3, 5, 31, 37], square [18, 21, 22, 38−40], lattice [23, 41−43] and X-structure [7], Y-structure [45] tried to be improved. Aluminum [3, 5, 25, 35, 37, 44−47] and carbon fiber [5, 7, 18, 20−23, 26, 33, 41−43, 48−52] cores were mostly preferred as core materials. As a result, by changing certain parameters such as material type, cell type, cell height and cover material of sandwich structures, the effect of these parameters on the specific strength under static and dynamic load was investigated.

In this study, unlike the literature, the effect of the core type under impact load was analyzed. For this purpose, sandwich structures with three different core types (square, egg box and lattice) were produced using completely composite materials. Instead of aluminum, aramid and paper (Nomex), which are widely used in the literature, layered carbon fiber composite was preferred as the core material in this study. Low-velocity impact tests were performed on the produced specimens and the effect of core type and size on impact strength was calculated. In addition to the experimental studies, numerical analyzes were carried out in the LS-DYNA finite element program under the same boundary conditions, using the MAT-162 material model, which allows progressive damage analysis. Fiber tensile damage, matrix compression damage, fiber compression damage and delamination damage that occurred after impact analysis were shown separately and compared with the experimental results.

2. MATERIALS AND METHOD

2.1. Experimental Study

The carbon fiber composite plates that make up the sandwich were purchased from Dost Kimya, Istanbul, Turkey. 245 gr/m^2 twill fabric and epoxy were used in its production. Composite plates consisting of 4 layers are 1 mm thick and the orientation angles of the composite plate are 0 . In order to obtain the three different core types shown in Fig. 1, the plates were cut using the water jet cutting method according to the sample properties given in Table 1. During cutting, great attention was paid to the material consumption in the composite plates, and the parts to be cut were placed on the plate in a way that minimized material loss. For the specimens named according to Table 1; The first letter indicates the core type; S: Square, E: Egg, L: Lattice, the following number indicates the cell height, and the last number indicates the total number of cells in the sample. The reason for choosing this type of core types is that the production technique is similar. Although the production technique of these three specimens is the

same, they have their own advantages and disadvantages. For example, the square cell structure has higher strength due to its high density. However, although the lattice structure is lighter, the production process is longer than the others. Therefore, thanks to this study, specific strength values depending on specific density were compared and their advantages over each other were presented. Interlocking technique was used to manufacture the core structure of the sandwich plate. In this technique, the slots cut with a water jet are clamped together with adhesive. Detailed measurements of the cores can be found in Bozkurt et al [53].

Since the produced specimen cores are of different types, their relative densities are different (Table 2). To calculate the relative densities of these lattice, egg box, and square structured specimens, the measurements in Equations (1)–(3) and [53] below were used, respectively [17, 55, 27]. The specific densities of the specimens are shown in Table 1.

$$\overline{\rho}_{lattice} = \frac{4btl + 4\left[(h_a + h_b)ct - cth_a\right]}{a^2 h}$$

1

$$\overline{\rho}_{egg} = \frac{d\left[(a + b - 2t)(H - h)c + 2ah - d\right]}{a^2 H}$$

2

$$\overline{\rho}_{square} = \frac{2t}{F}$$

3

The density of carbon fiber composites is 1500 kg/m^3. Therefore, the densities of the produced core structure were also calculated and given in Table 1. After the manufacturing of the core structures, the face sheets of the core structure were bonded. Face sheets have a size of 100x100 mm^2 for all specimens. Araldite 2015 was used as the adhesive material in the bonding process. After the gluing process, the assembly process was carried out by clamping it with the help of a vise so that there was no gap between the face sheet and the core structure, as seen in Fig. 2. After this process, the specimens were kept at room temperature for 24 hours for curing. For the weight drop test, a total of 30 specimens were produced, three from each specimen type given in Table 1. The low-velocity impact tests performed in this study were performed on the CEAST Fracovis Plus brand test device located in Adıyaman University Mechanical Engineering Laboratory (Fig. 3). Impact tests were performed according to ASTM D7136 standards [55]. A hemispherical striker was used during the tests. The diameter of the striking tip is 20 mm and its weight is 5.5 kg. According to 30 J impact energy, the velocity of the striker at the moment of impact is 3.332 m/s.

As seen in Table 3, the impact test was applied to the center of all specimens. The upper and lower adhesion surface area of the square structure is equal to each other and is 10 cm^2. In the lattice system,

this value is 2 cm^2. In the egg box, the lower adhesion surface area is 10 cm^2 and the upper surface contacted by the striker is 2.5 cm^2. In square and egg box specimens, the impact point is supported by the core cell walls. However, in the lattice structure, there is no cell wall at the impact point. This is due to the fact that although the cell base is the same, the cores geometries are different. In practical applications, the impact can occur in a sandwich structure in an arbitrary coordinate and with an arbitrary striker geometry. It is clear that the square cell structure is higher in terms of compressive strength than the other two types in relation to its specific density. Therefore, the resistance to impact will be higher. However, here we wanted to examine the damage response of these three types of core with the same cell number and base area to low-velocity impact [53].

2.2. Numerical Study

LS-DYNA, a finite element software, was used to analyze the impact response of sandwich specimens, and MAT-162 material card was used for progressive analysis [56]. The upper and lower holders are fixed supported to ensure the same boundary conditions as the experimental test setup (Fig. 4).
The striker, on the other hand, is constrained for displacements in the x and y directions and is only allowed to move in the batter's direction (z-axis). In this modeling, a total of 47825 nodes and 41654 solid elements were used using the 8-node solid element type. Two layers were used to define delamination [57]. Circular supports were modeled with a total of 3278 nodes and 3021 solid elements. The finite element model of the specimens to be tested is presented in Table 4. For progressive failure analysis in composite materials, element size throughout the thickness is of great importance [57]. In the low-velocity impact analysis performed on the square-core specimen, an optimization study was carried out by reducing the element height of the specimens from 1 mm to 0.2 mm throughout the thickness. Accordingly, the optimum element thickness was determined as 0.33 mm (Fig. 5).
The material parameters required to define the MAT-162 material model into the program are presented in Table 5. Among these parameters, $C_{AM1}, C_{AM2}, C_{AM3}, C_{AM4}, E_{LIMT}, E_{EXPN}$ and E_{CRSH} were calibrated and found by comparing experimental and numerical results [58]. φ, SF_{FC} and Ω_{MX} are taken from studies in the literature [57]. All remaining parameters were obtained as a result of experimental tests performed according to the standards specified in Table 6. MAT-162 material model is based on Hashin's [59] progressive failure principle and Matzenmiller et al. [60] is based on damage mechanics. This material model is used to model the progressive failure that occurs in composite layers subjected to high strain rate and high-pressure loading conditions. In the progressive damage model, the onset of damage is governed by equations. Equations for different damage types are given in Equations 4−10. Here, damage starts when the damage threshold is $r_i = 1, (i = 7, \ldots, 13)$. According to this; Tensile/shear damage in the direction parallel to and perpendicular to the fiber is given by the quadratic interaction between normal and through-thickness shear strain rates [61].

$$\left(\frac{E_x \cdot \epsilon_x}{S_{xT}}\right)^2 + \left(\frac{G_{xz} \cdot \epsilon_{xz}}{S_{FS}}\right)^2 - r_7{}^2 = 0 \text{ (in direction } x) \text{ (4)}$$

$$\left(\frac{E_y \cdot \epsilon_y}{S_{yT}}\right)^2 + \left(\frac{G_{yz} \cdot \epsilon_{yz}}{S_{FS}}\right)^2 - r_8{}^2 = 0 \text{ (in direction } y) \text{ (5)}$$

Here, ϵ_x and ϵ_y, refer to the axial strain changes in the x and y directions, respectively, and ϵ_{xz} and ϵ_{yz} refer to the shear strain changes in the $x - z$ and $y - z$ planes. It is assumed that the in-plane compression damage in the direction parallel to the fiber and perpendicular to the fiber is given by the maximum deformation criterion.

$$\left(\frac{E_x . \epsilon'_x}{S_{xC}}\right)^2 - r_9{}^2 = 0 \,, \epsilon'_x = -\epsilon_x - \langle \epsilon_z \rangle \frac{E_z}{E_x} = 0 \text{ (in direction } x) \text{ (6)}$$

$$\left(\frac{E_y . \epsilon'_y}{S_{yC}}\right)^2 - r_{10}{}^2 = 0 \,, \epsilon'_y = -\epsilon_y - \langle \epsilon_z \rangle \frac{E_z}{E_x} = 0 \text{ (in direction } y) \text{ (7)}$$

Crushing damage resulting from high thickness compression pressure was modeled using the following criterion.

$$\left(\frac{E_z . \epsilon_z}{S_{FC}}\right)^2 - r_{11}{}^2 = 0$$

8

$$\left(\frac{G_{xy} . \epsilon_{xy}}{S_{xy}}\right)^2 - r_{12}{}^2 = 0$$

9

Criterion for delamination damage mode;

$$\left(\bar{S}\right)^2 = \left\{ \left(\frac{E_z \langle \epsilon_z \rangle}{S_{zT}}\right)^2 + \left(\frac{G_{yz} . \epsilon_{yz}}{S_{yz0} + S_{SRC}}\right)^2 + \left(\frac{G_{zx} . \epsilon_{zx}}{S_{zx0} + S_{SRC}}\right)^2 \right\} - r_{13}{}^2 = 0$$

10

It is written as. S_{yz0} and S_{zx0} are quasi static shear strengths. $\bar{S}$, is the factor that takes into account the effect of stress concentration on the growth of delamination.S_{SRC}

$$S_{SRC} = -\epsilon_z . E_z . \tan\varphi$$

11

It is calculated with. Progressive damage is evaluated by six damage variables $\bar{\omega}_i, (i = 1, \ldots, 6)$, which result from damage in different modes and deteriorate the composite stiffness [62]. The damage model proposed by Matzenmiller [60] is the compliance matrix of the damaged state as in Eq. (12).

$$[S] = \begin{bmatrix} \dfrac{1}{\left(1-\bar{\omega}_1\right)E_x} & \dfrac{-\nu_{yx}}{E_y} & \dfrac{-\nu_{zx}}{E_z} & 0 & 0 & 0 \\[2ex] \dfrac{-\nu_{xy}}{E_x} & \dfrac{1}{\left(1-\bar{\omega}_2\right)E_y} & \dfrac{-\nu_{zy}}{E_z} & 0 & 0 & 0 \\[2ex] \dfrac{-\nu_{xz}}{E_x} & \dfrac{-\nu_{yz}}{E_y} & \dfrac{1}{\left(1-\bar{\omega}_3\right)E_z} & 0 & 0 & 0 \\[2ex] 0 & 0 & 0 & \dfrac{1}{\left(1-\bar{\omega}_4\right)G_{xy}} & 0 & 0 \\[2ex] 0 & 0 & 0 & 0 & \dfrac{1}{\left(1-\bar{\omega}_5\right)G_{yz}} & 0 \\[2ex] 0 & 0 & 0 & 0 & 0 & \dfrac{1}{\left(1-\bar{\omega}_6\right)G_{zx}} \end{bmatrix}$$

12

It is defined by. This matrix is used to reduce specific material mechanical properties according to each damage criterion. It is proposed in MAT-162 as an exponential function of strain rate as follows.

$$\left(\bar{\omega}_i\right) = 1 - \exp\left[\frac{1}{C_{AM}}\left(1 - r_j^{C_{AM}}\right)\right], r_j \geq 1$$

13

A *contact-eroding-surface-to-surface* contact card was used to model the interaction between the composite structure and the striker. *contact-automatic-surface-to-surface* model is used between the composite plate and the upper and lower holder. The dynamic friction coefficient between the striker and the composite material is 0.5 and the static friction coefficient is 0.3. Similarly, the friction coefficients between the holders and plates were taken as 0.6 and 0.4. The *contact-automatic-surface-to-surface-tiebreak* contact card was used to define the contact between the core structure and the upper and lower covers. Contact according to this card,

$$\left(\frac{|\sigma_n|}{NFLS}\right)^2 + \left(\frac{|\sigma_s|}{SFLS}\right)^2 \geq 1$$

14

It is broken by the condition. Here, σ_n and σ_s are the normal and shear stresses present, while $NFLS$ and $SFLS$ are the interface normal and shear strengths, respectively. Contact parameters for Araldite 2015 used as adhesive in this study are given in Table 7.

3. RESULTS AND DISCUSSION

Experimental and numerical low-velocity impact tests were carried out to examine the effect of core type and size on the impact strength and damage behavior of sandwich composites with square, egg box and

lattice core structures. Figure 6 shows the force-time, force-displacement and absorbed energy-time graphs for the 16-cell S15-16 specimen. The height of these specimens is 15 mm. In the contact force-time graph in Fig. 6a, the force reached the maximum point and then started to decrease. Accordingly, crushing and fracture damage occurred on the upper surface cover and face sheets after the peak impact load [63]. This situation is seen as a sudden decrease in force in the force-displacement graphs in Fig. 6b [7]. The impactor rebounded from the specimen surface and it was observed that the displacement value was zero at the end of the impact. In the absorbed energy-time graph in Fig. 6c, it is seen that some of the energy is absorbed and transferred to the specimen. For specimen S15-16, the minimum approximation ratio between experimental and numerical results is 91.23%. The production of the core using the interlocking technique and the subsequent gluing of the cover material was carried out entirely by hand. These small differences in the test results were interpreted as human-caused production errors [7].

Figure 7 shows the force-time, force-displacement and absorbed energy-time graphs of the E15-16 specimen after the 30 J impact test. In the force-time graph in Fig. 9a, it is seen that the maximum contact force obtained is lower than the square core type. However, it is evident that the displacement is greater after the impact (Fig. 7b). The contact force reached its peak value due to the impact between the striker and the upper face sheet. Crushing and fracture damage occurred in the upper face sheet and core after the peak impact load [64]. As seen in the contact force-displacement graph, these damages caused the fall [65]. When the striker pierced the upper face sheet and contacted the lower face sheet layer, the force increased again (Fig. 7a, b). The striker stopped after piercing the upper face sheet and touching the lower face sheet, and then the force reached zero. Therefore, this situation can be defined as penetration. It can be seen in the graph that the second peak value of the force is lower than the first value. Accordingly, the hitter lost some of his energy at the moment of first contact with the upper face sheet. Therefore, it hit the lower face sheet with a lower energy [63]. Figure 8 shows force-time, force-displacement and absorbed energy-time graphs for L15-16. The lattice structure is not strong enough to absorb 30 J compared to the other two types of core structures. For this reason, the impact energy applied in the tests was reduced to 10 J (Fig. 8a). According to Fig. 8c, in the force-displacement graph, the contact force between the striker and the upper face sheet due to the impact reached the peak value and then decreased to zero. In other words, the striker rebounded after hitting the specimen surface [66].

Figure 9 shows the effect of a specimen height increase on absorbed kinetic energy, maximum contact force and maximum displacement in 16-cell specimens with square core structure. These specimens were subjected to impact testing with 30 J. While the absorbed energies are normalized; First, the largest energy in three different sandwich structures was determined, and then all the energies in the graph were divided by this value (Fig. 9a). The amount of energy absorbed increases as the height increases [21]. However, according to Fig. 9b, it is seen that the maximum contact forces decrease as the core height increases. Additionally, the highest displacement occurred in the largest specimen with core height of 12.93 mm [21] (Fig. 9c). Similarly, Fig. 10 shows the effects of cell height on impact parameters in sandwiches with lattice core structure. There is an increase in absorption energy if it increases from $h = 20$ mm to $h = 30$ mm. However, this increase is not as obvious as in the square core type. The highest value was obtained at $h = 15$ mm.

Considering the error bars, it can be said that the height effect is around 10% (Fig. 10a). It is seen that the maximum contact force decreases as the core height increases. In lattice sandwich structures with different heights exposed to the same impact energy, the highest displacement occurred in the specimen with the largest core height of 14.14 mm, again similar to the square core type [66]. The main damage modes of the sandwich structure can be interlamination on the face sheets, matrix and fiber damage, as well as bending or fracture of the core structure. At low impact energy, the most widespread damage pattern in the upper face sheet around the impact zone is interlayer delamination. As the impact energy increases, intra-laminar damages such as fiber breakage and matrix cracking resulting from failure will replace inter-laminar delamination for the low impact energy case [7]. In Fig. 11, the transverse matrix damage areas are compared numerically and experimentally for the S15-16, E15-16 and L15-16 specimens, respectively, after the impact test. The first surface that the striker comes into contact with at the time of impact is given as front view. The surface remaining on the underside of the contact surface is shown as the back view. When the graphs are examined, it can be seen that the transverse matrix damage areas are compatible with each other. For E15-16, damage occurred to the lower face sheet along with the upper face sheet due to the impact of the strike, while for S15-16 and L15-16, only the upper face sheet was damaged.

Damage morphologies are shown in numerical detail in Table 8. In this table, the regions shown in red in the LS-DYNA numerical results are the regions where damage occurred. When the impact damage patterns are examined, it is seen that crushing and breaking damage occurs in the upper face sheet and the cell wall supporting it from below due to the impact of the impact. In the case of the in-plane matrix, it can be seen that the red area where the damage occurs is greater than the other damage types.

According to Fig. 12a, the maximum contact forces for the egg box core structure when the number of cells is 4 and 16 are 2854 N and 3293 N, respectively. It is seen that the maximum contact force decreases as the core width increases, that is, the number of cells decreases [21]. Therefore, as the cell density increases, the impact resistance of the sandwich structure also increases [54]. However, specific maximum contact forces were obtained by dividing the maximum contact force values for both cell types by their respective densities. In this case, when the contact forces were examined, it was seen that the results were close to each other as expected. In Fig. 12b, the maximum contact forces of square and egg box core type specimens are specifically compared. Because although the number of cells, base area and height are the same for each cores type, it can be seen in Table 1 that their specific densities are different. Since the core wall types are different, it is not possible to use a common specific density. Therefore, only when specific contact forces are compared can it be seen that the egg box has a higher value.

In Fig. 13, the percentage absorbed energy of specimens produced in lattice and square core types is presented for different cell heights. When 30 J impact energy was applied to the S15-16 specimen, it absorbed 85% of its energy. For specimen L15-16, this value is 80%. Egg box specimens (E15-16, E20-16) absorbed all the energy due to penetration by the striker in case of impact, and this situation is not shown in the graph. Similar behaviors were obtained in the comparisons made for $h = 20$ and 30 sandwich height (Fig. 13b, c).

In Fig. 14, the vertical axis is obtained by dividing the percentage of energy absorbed by the sandwich by its own density. The horizontal axis shows the relative density. Although the energy absorption ability of the low-density carbon lattice cores used in the study according to relative density is lower than the square core sandwich structures, it is similar ([67], [69]) or even superior ([17]) to other lightweight lattice cores with similar density in the literature., [70]) can be seen. Zhang et al. [17] used aluminum lattice core in their study. According to Fig. 14, when the percentage energy absorption per unit density of the sandwich composite made entirely of carbon fiber is compared with aluminum, it can be said that the performance of the sandwich structure presented in this study is successful, considering the density.

After-impact force-time, force-displacement and energy-time graphs of square-section sandwich composite structures with different face sheet thicknesses, using models verified by experimental and numerical results, are shown numerically only in Fig. 15. According to this; When the force-time graph is examined, when the face sheet thickness is t = 0.5 mm, a perforation occurs in the specimen after the striker contacts the specimen, and due to the ongoing friction between the striker and the sandwich plate, the contact force remained constant at a certain value and did not decrease to zero. When the face sheet thickness was t = 1 and 1.5 mm, rebounding occurred on the striking specimen surface. Therefore, as the face sheet thickness increases, the amount of displacement in the specimen decreases as the rigidity of the sample increases [21]. The maximum contact force when the face sheet thicknesses were t = 0.5 and 1.5 mm was determined as 4567 N and 7219 N, respectively. It is observed that the maximum contact force increases as the valve thickness increases [21]. The sample with t = 1 mm face sheet thickness absorbed 18% more energy than t = 1.5.

When the impact damage patterns are examined in Table 9, it is seen that fracture damage occurred in the top cover and core due to the impact of the impact in the specimen with cover thickness t = 0.5 mm. The striker penetrated the upper face sheet and the core structure and passed to the lower face sheet. Here, perforation is seen due to impact. Figure 15b shows that there is no rebound in the striker and it proceeds by piercing the specimen. In other surface face sheet thicknesses, the striker bounced back without piercing the top face sheet.

4. CONCLUSION

This study examined the low-velocity impact response of carbon fiber sandwich composites with square, egg box and lattice core structures. All three types of core structures are produced with the interlocking technique. Strength values were calculated experimentally and numerically by applying a weight drop test to the produced specimens. The results obtained can be summarized as follows::

- Increasing the cell height reduces the maximum contact force. After the impact test performed for 30 J, while the striker rebounded in the square core, it pierced the sandwich structure in the egg box. If it is the same value, the lattice core is completely damaged.
- For a 16-cell egg carton cell, a 4-times increase in density increased the maximum force at 30 J by 15%. When specific loads are compared using a square core sample under the same conditions, it can be said that the contact force of the egg box structure is higher.

- If the absorbed energy is compared as a percentage, it is seen that the energy absorption of the square core structure is higher than the lattice structure.
- Numerical analyzes for the low-velocity impact test were obtained with a minimum approximation rate of 82% through experimental measurements. This numerical model shows that it can be a helpful tool in the development of new, lightweight, multifunctional and complex structures for many engineering applications. For this purpose, as a result of the analyzes made without experimenting, it was determined that increasing the face sheet thickness by 2 times for a square structure increased the maximum contact force by 58%.
- It is seen that the impact mechanical properties of sandwich core structures depend on the geometry and material of the core materials as well as the relative density of the core structure. The square core structure has the ability to absorb partially more energy for higher specific density than the egg and lattice. It has been determined that these produced sandwiches have similar or higher energy absorption capabilities than other lightweight lattice cores with similar relative density in the literature. It can be said that the sandwich lattice structure performance presented in this study is successful compared to the aluminum core structure, considering the density. Because if aluminum is used with the same geometry, the density of these cores will increase by 1.8 times. At this point, designers need to pay attention to the density/% absorbed energy ratio of sandwiches.

Declarations

References

1. W. He, J. Liu, B. Tao, D. Xie, J. Liu, ve M. Zhang, "Experimental and numerical research on the low velocity impact behavior of hybrid corrugated core sandwich structures", *Compos. Struct.*, c. 158, ss. 30–43, 2016, doi: 10.1016/j.compstruct.2016.09.009.
2. B. Wang, L. Z. Wu, L. Ma, ve J. C. Feng, "Low-velocity impact characteristics and residual tensile strength of carbon fiber composite lattice core sandwich structures", *Compos. Part B Eng.*, c. 42, sayı

4, ss. 891–897, 2011, doi: 10.1016/j.compositesb.2011.01.007.

3. I. Ivañez ve S. Sanchez-Saez, "Numerical modelling of the low-velocity impact response of composite sandwich beams with honeycomb core", *Compos. Struct.*, c. 106, ss. 716–723, 2013, doi: 10.1016/j.compstruct.2013.07.025.

4. C. Zhang ve K. T. Tan, "Low-velocity impact response and compression after impact behavior of tubular composite sandwich structures", *Compos. Part B Eng.*, c. 193, sayı January, s. 108026, 2020, doi: 10.1016/j.compositesb.2020.108026.

5. J. Liu, W. He, D. Xie, ve B. Tao, "The effect of impactor shape on the low-velocity impact behavior of hybrid corrugated core sandwich structures", *Compos. Part B Eng.*, c. 111, ss. 315–331, 2017, doi: 10.1016/j.compositesb.2016.11.060.

6. W. He, L. Yao, X. Meng, G. Sun, D. Xie, ve J. Liu, "Effect of structural parameters on low-velocity impact behavior of aluminum honeycomb sandwich structures with CFRP face sheets", *Thin-Walled Struct.*, c. 137, sayı August 2018, ss. 411–432, 2019, doi: 10.1016/j.tws.2019.01.022.

7. W. He, J. Liu, S. Wang, ve D. Xie, "Low-velocity impact behavior of X-Frame core sandwich structures – Experimental and numerical investigation", *Thin-Walled Struct.*, c. 131, sayı July, ss. 718–735, 2018, doi: 10.1016/j.tws.2018.07.042.

8. D. Feng ve F. Aymerich, "Effect of core density on the low-velocity impact response of foam-based sandwich composites", *Compos. Struct.*, c. 239, sayı January, s. 112040, 2020, doi: 10.1016/j.compstruct.2020.112040.

9. X. Zhang, F. Xu, Y. Zang, ve W. Feng, "Experimental and numerical investigation on damage behavior of honeycomb sandwich panel subjected to low-velocity impact", *Compos. Struct.*, c. 236, sayı January, s. 111882, 2020, doi: 10.1016/j.compstruct.2020.111882.

10. Y. Wan, C. Diao, B. Yang, L. Zhang, ve S. Chen, "GF/epoxy laminates embedded with wire nets: A way to improve the low-velocity impact resistance and energy absorption ability", *Compos. Struct.*, c. 202, sayı 130, ss. 818–835, 2018, doi: 10.1016/j.compstruct.2018.04.041.

11. W. He, J. Liu, S. Wang, ve D. Xie, "Low-velocity impact response and post-impact flexural behaviour of composite sandwich structures with corrugated cores", *Compos. Struct.*, c. 189, sayı January, ss. 37–53, 2018, doi: 10.1016/j.compstruct.2018.01.024.

12. W. He, S. Lu, K. Yi, S. Wang, G. Sun, ve Z. Hu, "Residual flexural properties of CFRP sandwich structures with aluminum honeycomb cores after low-velocity impact", *Int. J. Mech. Sci.*, c. 161–162, sayı July, s. 105026, 2019, doi: 10.1016/j.ijmecsci.2019.105026.

13. Q. Wu, L. Ma, L. Wu, ve J. Xiong, "A novel strengthening method for carbon fiber composite lattice truss structures", *Compos. Struct.*, c. 153, ss. 585–592, 2016, doi: 10.1016/j.compstruct.2016.06.060.

14. S. Hou, S. Zhao, L. Ren, X. Han, ve Q. Li, "Crashworthiness optimization of corrugated sandwich panels", *Mater. Des.*, c. 51, ss. 1071–1084, 2013, doi: 10.1016/j.matdes.2013.04.086.

15. T. Boonkong, Y. O. Shen, Z. W. Guan, ve W. J. Cantwell, "The low velocity impact response of curvilinear-core sandwich structures", *Int. J. Impact Eng.*, c. 93, ss. 28–38, 2016, doi: 10.1016/j.ijimpeng.2016.01.012.

16. D. D. Radford, N. A. Fleck, ve V. S. Deshpande, "The response of clamped sandwich beams subjected to shock loading", *Int. J. Impact Eng.*, c. 32, sayı 6, ss. 968–987, 2006, doi: 10.1016/j.ijimpeng.2004.08.007.

17. G. Zhang, B. Wang, L. Ma, J. Xiong, ve L. Wu, "Response of sandwich structures with pyramidal truss cores under the compression and impact loading", *Compos. Struct.*, c. 100, ss. 451–463, 2013, doi: 10.1016/j.compstruct.2013.01.012.

18. V. Crupi, E. Kara, G. Epasto, E. Guglielmino, ve H. Aykul, "Prediction model for the impact response of glass fibre reinforced aluminium foam sandwiches", *Int. J. Impact Eng.*, c. 77, ss. 97–107, 2015, doi: 10.1016/j.ijimpeng.2014.11.012.

19. A. C. Balaban, K. F. Tee, ve M. E. Toygar, "Low velocity impact behaviour of sandwich composite structures with E-glass/epoxy facesheets and PVC foam", *Procedia Struct. Integr.*, c. 18, ss. 577–585, 2019, doi: 10.1016/j.prostr.2019.08.202.

20. S. Jiang, F. Sun, X. Zhang, ve H. Fan, "Interlocking orthogrid: An efficient way to construct lightweight lattice-core sandwich composite structure", *Compos. Struct.*, c. 176, ss. 55–71, 2017, doi: 10.1016/j.compstruct.2017.05.029.

21. X. Xue, C. Zhang, W. Chen, M. Wu, ve J. Zhao, "Study on the impact resistance of honeycomb sandwich structures under low-velocity/heavy mass", *Compos. Struct.*, c. 226, sayı May, s. 111223, 2019, doi: 10.1016/j.compstruct.2019.111223.

22. T. George, V. S. Deshpande, ve H. N. G. Wadley, "Mechanical response of carbon fiber composite sandwich panels with pyramidal truss cores", *Compos. Part A Appl. Sci. Manuf.*, c. 47, sayı 1, ss. 31–40, 2013, doi: 10.1016/j.compositesa.2012.11.011.

23. L. J. Feng, Z. T. Yang, G. C. Yu, X. J. Chen, ve L. Z. Wu, "Compressive and shear properties of carbon fiber composite square honeycombs with optimized high-modulus hierarchical phases", *Compos. Struct.*, c. 201, sayı March, ss. 845–856, 2018, doi: 10.1016/j.compstruct.2018.06.080.

24. J. Wang, A. M. Waas, ve H. Wang, "Experimental and numerical study on the low-velocity impact behavior of foam-core sandwich panels", *Compos. Struct.*, c. 96, ss. 298–311, 2013, doi: 10.1016/j.compstruct.2012.09.002.

25. S. Heimbs, J. Cichosz, M. Klaus, S. Kilchert, ve A. F. Johnson, "Sandwich structures with textile-reinforced composite foldcores under impact loads", *Compos. Struct.*, c. 92, sayı 6, ss. 1485–1497, 2010, doi: 10.1016/j.compstruct.2009.11.001.

26. G. Zhu, G. Sun, G. Li, A. Cheng, ve Q. Li, "Modeling for CFRP structures subjected to quasi-static crushing", *Compos. Struct.*, c. 184, ss. 41–55, 2018, doi: 10.1016/j.compstruct.2017.09.001.

27. S. Park, B. P. Russell, V. S. Deshpande, ve N. A. Fleck, "Dynamic compressive response of composite square honeycombs", *Compos. Part A Appl. Sci. Manuf.*, c. 43, sayı 3, ss. 527–536, 2012, doi: 10.1016/j.compositesa.2011.11.022.

28. Y. Hu, W. Li, X. An, ve H. Fan, "Fabrication and mechanical behaviors of corrugated lattice truss composite sandwich panels", *Compos. Sci. Technol.*, c. 125, ss. 114–122, 2016, doi: 10.1016/j.compscitech.2016.02.003.

29. A. Akatay, M. Ö. Bora, O. Çoban, S. Fidan, ve V. Tuna, "The influence of low velocity repeated impacts on residual compressive properties of honeycomb sandwich structures", *Compos. Struct.*, c. 125, ss. 425–433, 2015, doi: 10.1016/j.compstruct.2015.02.057.

30. Y. Chen, S. Hou, K. Fu, X. Han, ve L. Ye, "Low-velocity impact response of composite sandwich structures: Modelling and experiment", *Compos. Struct.*, c. 168, ss. 322–334, 2017, doi: 10.1016/j.compstruct.2017.02.064.

31. A. Kurşun, M. Şenel, H. M. Enginsoy, ve E. Bayraktar, "Effect of impactor shapes on the low velocity impact damage of sandwich composite plate: Experimental study and modelling", *Compos. Part B Eng.*, c. 86, ss. 143–151, 2016, doi: 10.1016/j.compositesb.2015.09.032.

32. B. B. Liao ve P. F. Liu, "Finite element analysis of dynamic progressive failure of plastic composite laminates under low velocity impact", *Compos. Struct.*, c. 159, ss. 567–578, 2017, doi: 10.1016/j.compstruct.2016.09.099.

33. O. T. Topac, B. Gozluklu, E. Gurses, ve D. Coker, "Experimental and computational study of the damage process in CFRP composite beams under low-velocity impact", *Compos. Part A Appl. Sci. Manuf.*, c. 92, ss. 167–182, 2017, doi: 10.1016/j.compositesa.2016.06.023.

34. M. R. Yellur, H. Seidlitz, F. Kuke, K. Wartig, ve N. Tsombanis, "A low velocity impact study on press formed thermoplastic honeycomb sandwich panels", *Compos. Struct.*, c. 225, sayı November 2018, s. 111061, 2019, doi: 10.1016/j.compstruct.2019.111061.

35. J. Zhang, K. Liu, Y. Ye, ve Q. Qin, "Low-velocity impact of rectangular multilayer sandwich plates", *Thin-Walled Struct.*, c. 141, sayı April, ss. 308–318, 2019, doi: 10.1016/j.tws.2019.04.033.

36. G. Morada, R. Ouadday, A. Vadean, ve R. Boukhili, "Low-velocity impact resistance of ATH/epoxy core sandwich composite panels: Experimental and numerical analyses", *Compos. Part B Eng.*, c. 114, ss. 418–431, 2017, doi: 10.1016/j.compositesb.2017.01.070.

37. Y. Wu, Q. Liu, J. Fu, Q. Li, ve D. Hui, "Dynamic crash responses of bio-inspired aluminum honeycomb sandwich structures with CFRP panels", *Compos. Part B Eng.*, c. 121, ss. 122–133, 2017, doi: 10.1016/j.compositesb.2017.03.030.

38. B. P. Russell, T. Liu, N. A. Fleck, ve V. S. Deshpande, "The soft impact of composite sandwich beams with a square-honeycomb core", *Int. J. Impact Eng.*, c. 48, ss. 65–81, 2012, doi: 10.1016/j.ijimpeng.2011.04.007.

39. J. Zhou, M. Z. Hassan, Z. Guan, ve W. J. Cantwell, "The low velocity impact response of foam-based sandwich panels", *Compos. Sci. Technol.*, c. 72, sayı 14, ss. 1781–1790, 2012, doi: 10.1016/j.compscitech.2012.07.006.

40. S. S. Shi, Z. Sun, X. Z. Hu, ve H. R. Chen, "Carbon-fiber and aluminum-honeycomb sandwich composites with and without Kevlar-fiber interfacial toughening", *Compos. Part A Appl. Sci. Manuf.*, c. 67, ss. 102–110, 2014, doi: 10.1016/j.compositesa.2014.08.017.

41. G. Sun, D. Chen, X. Huo, G. Zheng, ve Q. Li, "Experimental and numerical studies on indentation and perforation characteristics of honeycomb sandwich panels", *Compos. Struct.*, c. 184, sayı August 2017, ss. 110–124, 2018, doi: 10.1016/j.compstruct.2017.09.025.

42. G. C. Yu, L. J. Feng, ve L. Z. Wu, "Thermal and mechanical properties of a multifunctional composite square honeycomb sandwich structure", *Mater. Des.*, c. 102, ss. 238–246, 2016, doi: 10.1016/j.matdes.2016.04.050.

43. H. Fan, F. Sun, L. Yang, F. Jin, ve D. Zhao, "Interlocked hierarchical lattice materials reinforced by woven textile sandwich composites", *Compos. Sci. Technol.*, c. 87, ss. 142–148, 2013, doi: 10.1016/j.compscitech.2013.07.028.

44. B. Wang, L. Wu, L. Ma, Y. Sun, ve S. Du, "Mechanical behavior of the sandwich structures with carbon fiber-reinforced pyramidal lattice truss core", *Mater. Des.*, c. 31, sayı 5, ss. 2659–2663, 2010, doi: 10.1016/j.matdes.2009.11.061.

45. J. Liu, J. Liu, J. Mei, ve W. Huang, "Investigation on manufacturing and mechanical behavior of all-composite sandwich structure with Y-shaped cores", *Compos. Sci. Technol.*, c. 159, ss. 87–102, 2018, doi: 10.1016/j.compscitech.2018.01.026.

46. A. Kurşun, M. Şenel, ve H. M. Enginsoy, "Experimental and numerical analysis of low velocity impact on a preloaded composite plate", *Adv. Eng. Softw.*, c. 90, ss. 41–52, 2015, doi: 10.1016/j.advengsoft.2015.06.010.

47. J. L. Yu, X. Wang, Z. G. Wei, ve E. H. Wang, "Deformation and failure mechanism of dynamically loaded sandwich beams with aluminum-foam core", *Int. J. Impact Eng.*, c. 28, sayı 3, ss. 331–347, 2003, doi: 10.1016/S0734-743X(02)00053-2.

48. Z. H. Tan, H. H. Luo, W. G. Long, ve X. Han, "Dynamic response of clamped sandwich beam with aluminium alloy foam core subjected to impact loading", *Compos. Part B Eng.*, c. 46, ss. 39–45, 2013, doi: 10.1016/j.compositesb.2012.10.044.

49. Y. Rong, J. Liu, W. Luo, ve W. He, "Effects of geometric configurations of corrugated cores on the local impact and planar compression of sandwich panels", *Compos. Part B Eng.*, c. 152, sayı August, ss. 324–335, 2018, doi: 10.1016/j.compositesb.2018.08.130.

50. C. Shu, S. Zhao, ve S. Hou, "Crashworthiness analysis of two-layered corrugated sandwich panels under crushing loading", *Thin-Walled Struct.*, c. 133, sayı July, ss. 42–51, 2018, doi: 10.1016/j.tws.2018.09.008.

51. J. Xiong, L. Ma, L. Wu, B. Wang, and A. Vaziri, "Fabrication and crushing behavior of low density carbon fiber composite pyramidal truss structures", *Compos. Struct.*, c. 92, sayı 11, ss. 2695–2702, 2010, doi: 10.1016/j.compstruct.2010.03.010.

52. J. Mei, J. Liu, J. Liu, J. Mei, J. Liu, ve J. Liu, "A novel fabrication method and mechanical behavior of all-composite tetrahedral truss core sandwich panel", *Compos. Part A Appl. Sci. Manuf.*, c. 102, ss. 28–39, 2017, doi: 10.1016/j.compositesa.2017.07.020.

53. Bozkurt, I., Kaman, M. O., and Albayrak, M. "Low-velocity impact behaviours of sandwiches manufactured from fully carbon fiber composite for different cell types and compression behaviours for different core types." *Materials Testing*, 2023

54. J. Xiong, A. Vaziri, R. Ghosh, H. Hu, L. Ma, ve L. Wu, "Compression behavior and energy absorption of carbon fiber reinforced composite sandwich panels made of three-dimensional honeycomb grid

cores", *Extrem. Mech. Lett.*, c. 7, ss. 114–120, 2016, doi: 10.1016/j.eml.2016.02.012.

55. D. ASTM International, *ASTM International, Designation: D7136/D7136M - 12 'Standard test method for measuring the damage resistance of a fiber-reinforced polymer matrix composite to a drop-weight impact event*, ASTM Inter., c. 1. 2012.

56. H. JO., *LS-DYNA Keyword User's Manual Volume II Material Models, Version 971. Livermore Software Technology Corporation; . [24]*. 2017.

57. B. Z. Haque, "MAT162-USER-MANUAL-Version-15A-2015", sayı 215, 2015.

58. İ. Bozkurt, M. Kaman, M. Albayrak, ve A. M. Bozkurt İ, Kaman MO, "LS-DYNA MAT162 Finding Material Inputs and Investigation of Impact Damage in Carbon Composite Plates. XVI. international research conference 2022.", ss. 3–7, 2022.

59. Z. Hashin, "Failure Criteria for Unidirectional Mr!", *J. Appl. Mech.*, c. 47, sayı June, ss. 329–334, 1980.

60. A. Matzenmiller, J. Lubliner, ve R. L. Taylor, "A constitutive model for anisotropic damage in fiber-composites", *Mech. Mater.*, c. 20, sayı 2, ss. 125–152, 1995, doi: 10.1016/0167-6636(94)00053-0.

61. J. R. Xiao, B. A. Gama, ve J. W. Gillespie, "Progressive damage and delamination in plain weave S-2 glass/SC-15 composites under quasi-static punch-shear loading", *Compos. Struct.*, c. 78, sayı 2, ss. 182–196, 2007, doi: 10.1016/j.compstruct.2005.09.001.

62. A. Vescovini *vd.*, "Numerical investigation on the hybridization effect in inter-ply S2-glass and aramid woven composites subjected to ballistic impacts", *Compos. Struct.*, c. 276, s. 114506, 2021, doi: 10.1016/j.compstruct.2021.114506.

63. Y. Chen, K. Fu, S. Hou, X. Han, ve L. Ye, "Multi-objective optimization for designing a composite sandwich structure under normal and 45° impact loadings", *Compos. Part B Eng.*, c. 142, sayı December 2016, ss. 159–170, 2018, doi: 10.1016/j.compositesb.2018.01.020.

64. S. H. Abo Sabah, A. B. H. Kueh, ve N. M. Bunnori, "Failure mode maps of bio-inspired sandwich beams under repeated low-velocity impact", *Compos. Sci. Technol.*, c. 182, sayı February, s. 107785, 2019, doi: 10.1016/j.compscitech.2019.107785.

65. S. H. Abo Sabah, A. B. H. Kueh, ve M. Y. Al-Fasih, "Comparative low-velocity impact behavior of bio-inspired and conventional sandwich composite beams", *Compos. Sci. Technol.*, c. 149, ss. 64–74, 2017, doi: 10.1016/j.compscitech.2017.06.014.

66. J. Xiong, A. Vaziri, L. Ma, J. Papadopoulos, ve L. Wu, "Compression and impact testing of two-layer composite pyramidal-core sandwich panels", *Compos. Struct.*, c. 94, sayı 2, ss. 793–801, 2012, doi: 10.1016/j.compstruct.2011.09.018.

67. "3D printed ABS material Low-Velocity Impact Behavior of Sandwich Structures with Additively Manufactured Polymer Lattice Cores _ Enhanced Reader.pdf". .

68. J. S. Yang *vd.*, "Low velocity impact behavior of carbon fibre composite curved corrugated sandwich shells", *Compos. Struct.*, c. 238, sayı August 2019, ss. 1–16, 2020, doi: 10.1016/j.compstruct.2020.112027.

69. G. Zhang, B. Wang, L. Ma, L. Wu, S. Pan, ve J. Yang, "Energy absorption and low velocity impact response of polyurethane foam filled pyramidal lattice core sandwich panels", *Compos. Struct.*, c. 108, sayı 1, ss. 304–310, 2014, doi: 10.1016/j.compstruct.2013.09.040.

70. M. F. Ashby, "The properties of foams and lattices", *Philos. Trans. R. Soc. A Math. Phys. Eng. Sci.*, c. 364, sayı 1838, ss. 15–30, 2006, doi: 10.1098/rsta.2005.1678.

Tables

Tables 1-9 are available in the Supplementary Files section.

Figures

a) b) c)
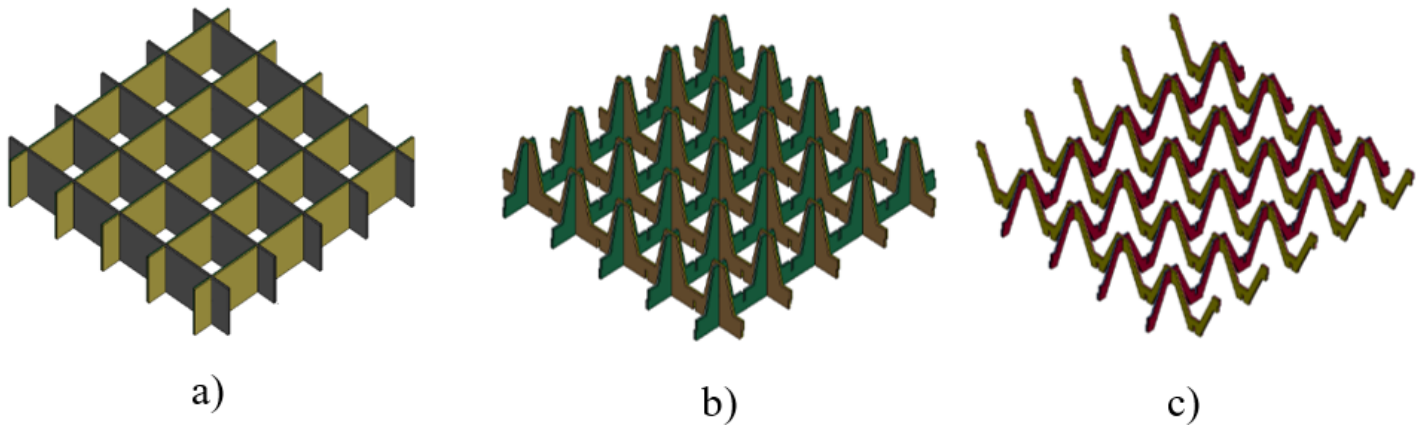
Figure 1

a) Square, b) egg and c) lattice core type.
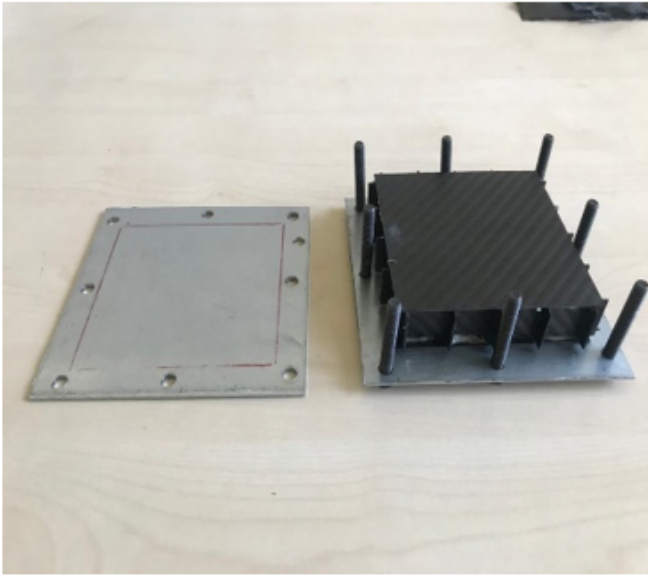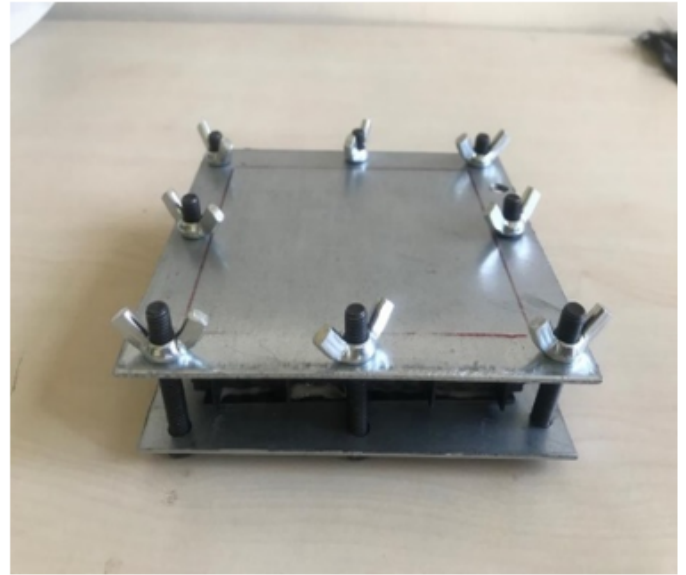
Figure 2

a) Gluing the core and face sheets b) placing them in the mold
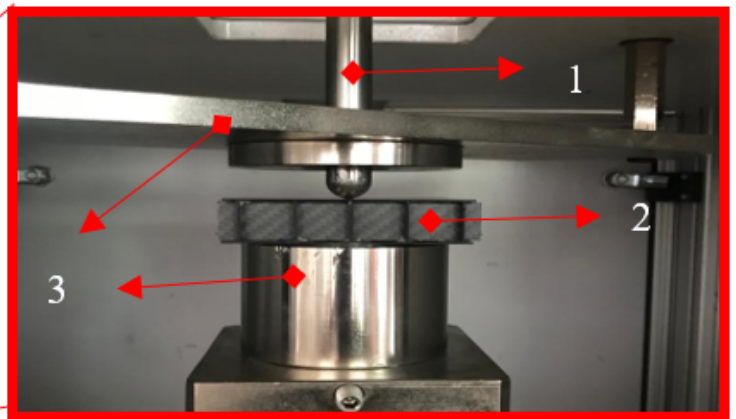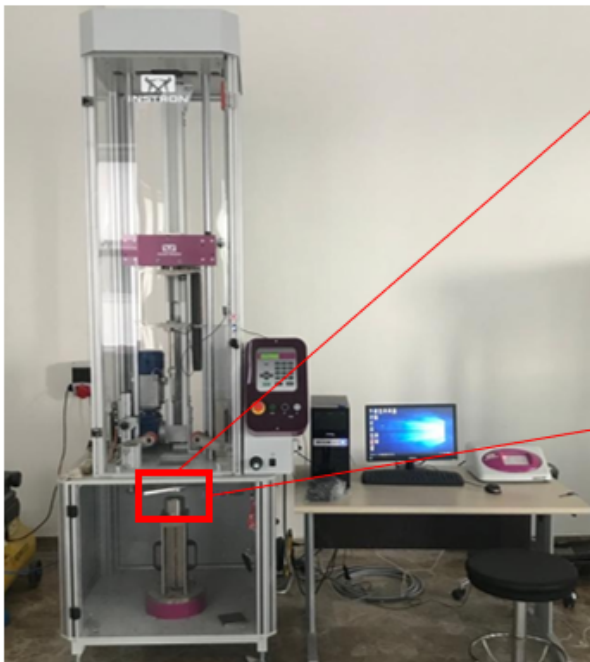
1. Striker
2. Specimen
3. Upper and lower holder

Figure 3

Low velocity impact test device

1-Striker
2- Upper and lower holder
3- Composite face sheets
4- Composite square core
5- Composite egg core
6- Composite lattice core
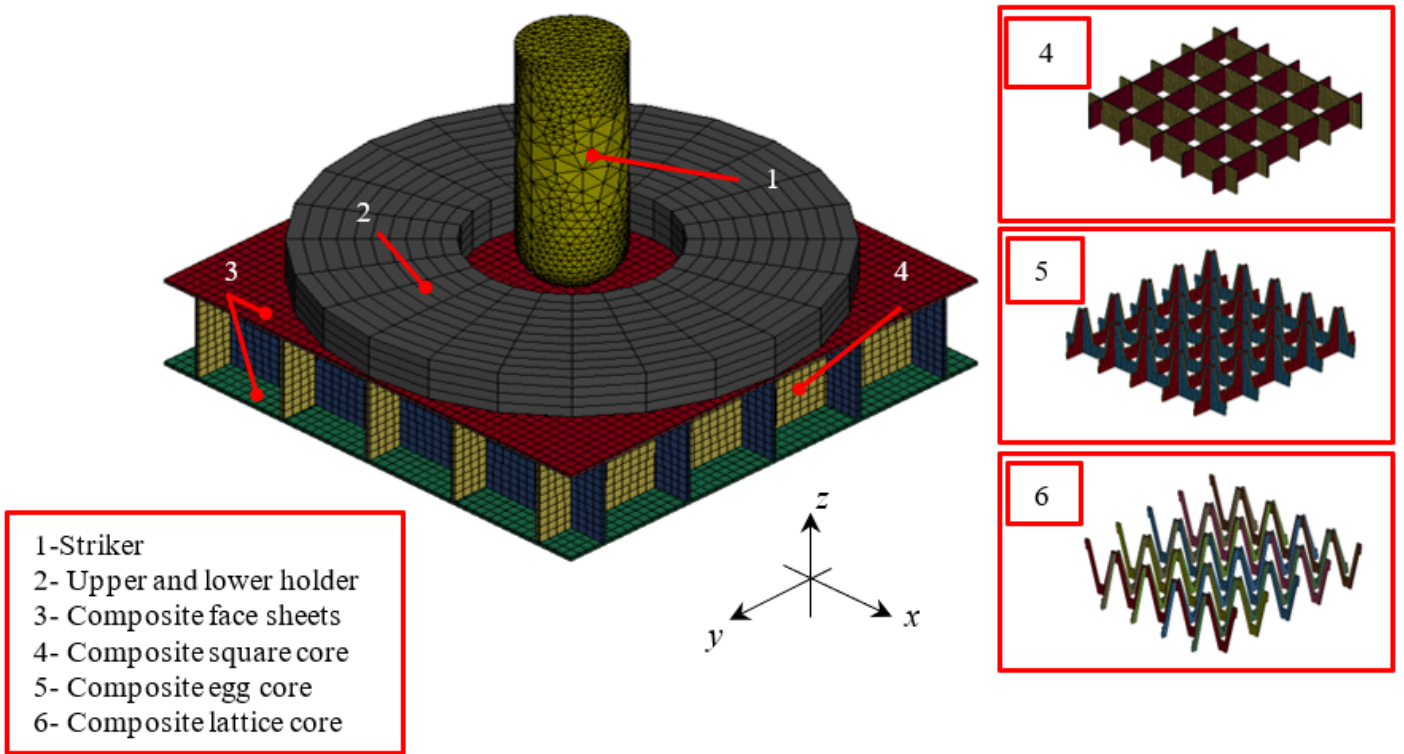
Figure 4

Finite element model of sandwich specimens for different cores.
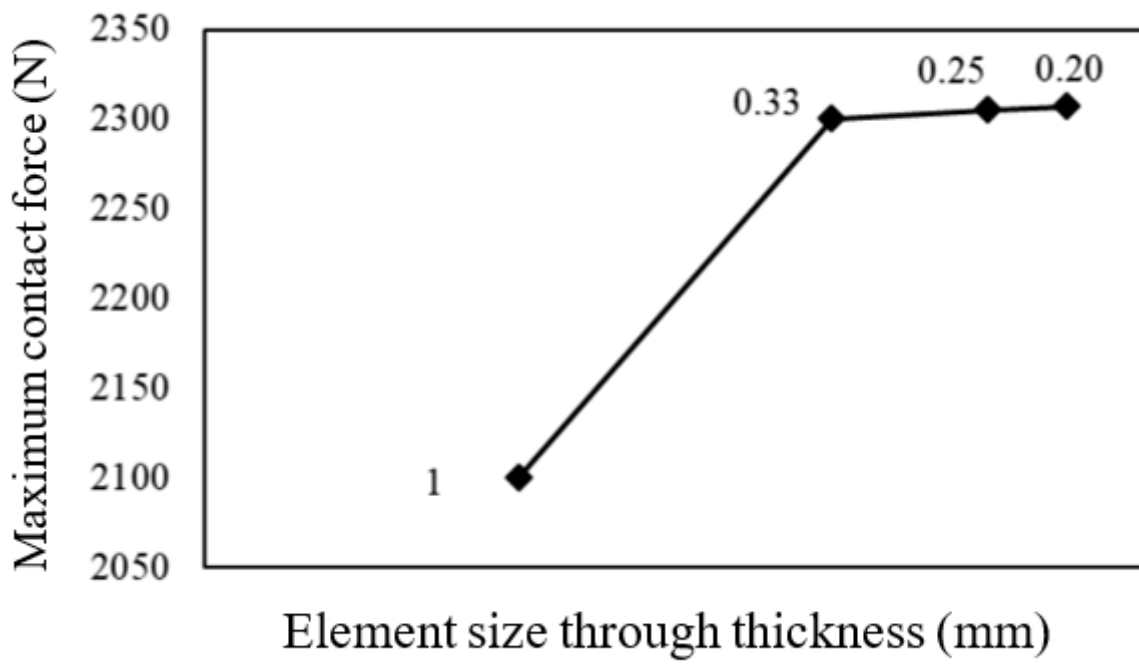
Figure 5

Mesh optimization across face sheet thickness for square core sandwich.

a)

b)

c)
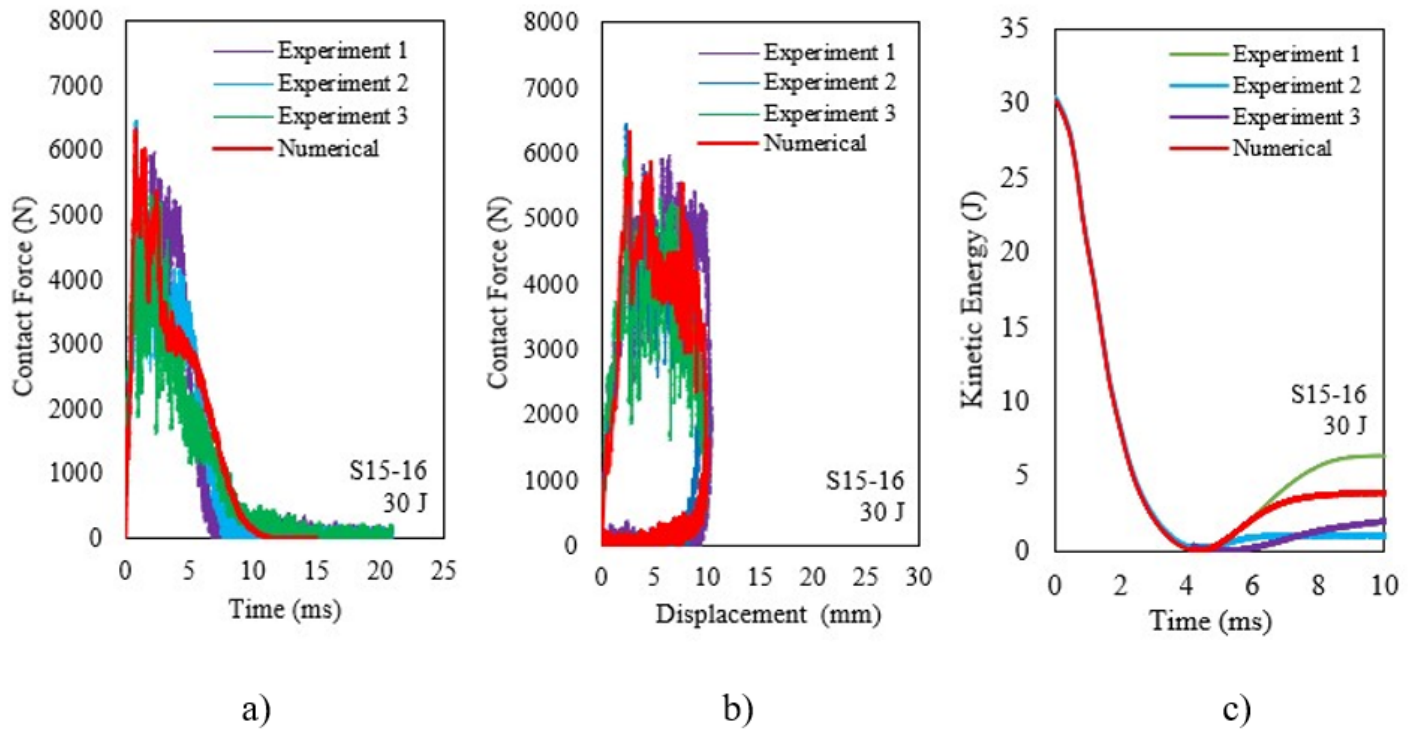
Figure 6

a) Contact force-time b) contact force -displacement c) kinetic energy-time graph for the S15-16.

a)

b)

c)
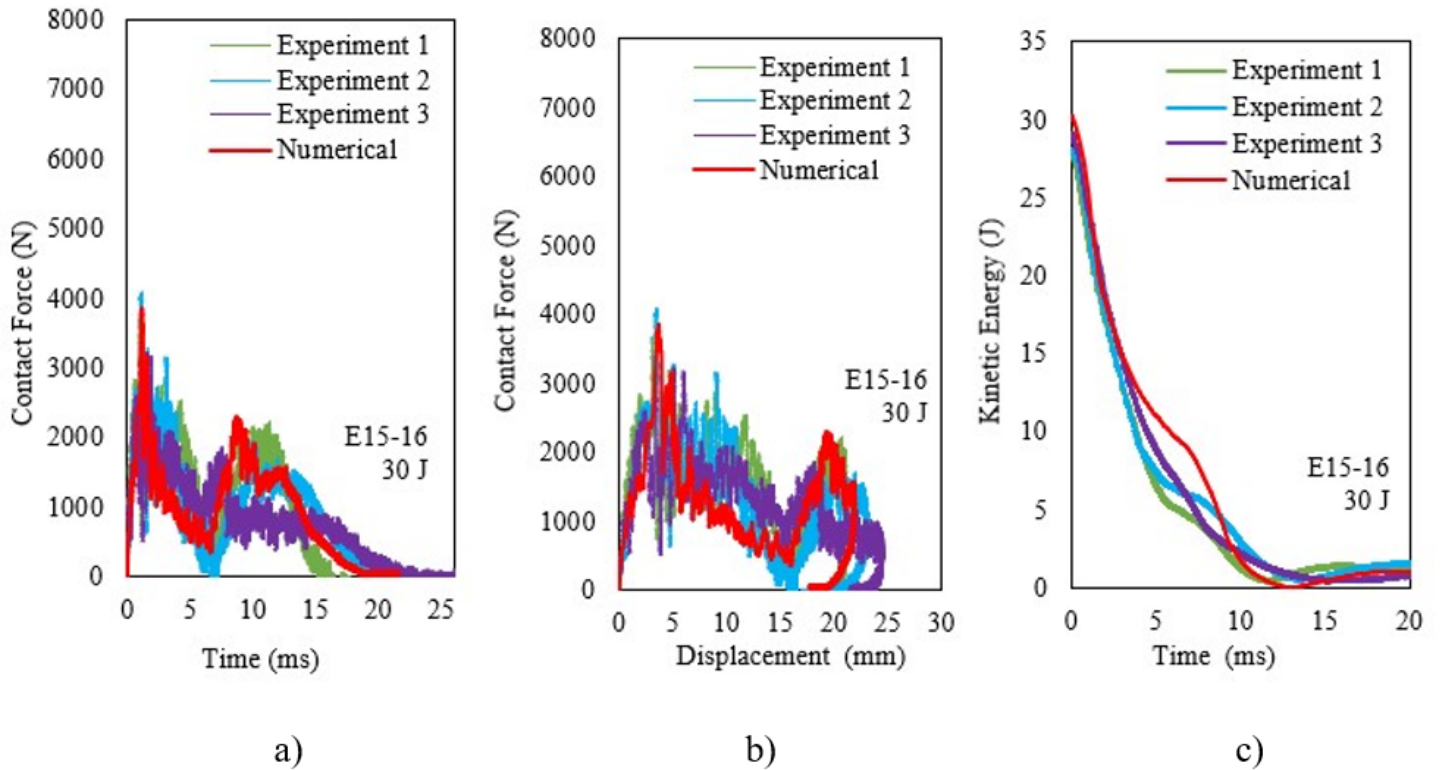
Figure 7

a) Contact force-time b) contact force -displacement c) kinetic energy-time graph for the E15-16.

a)

b)

c)
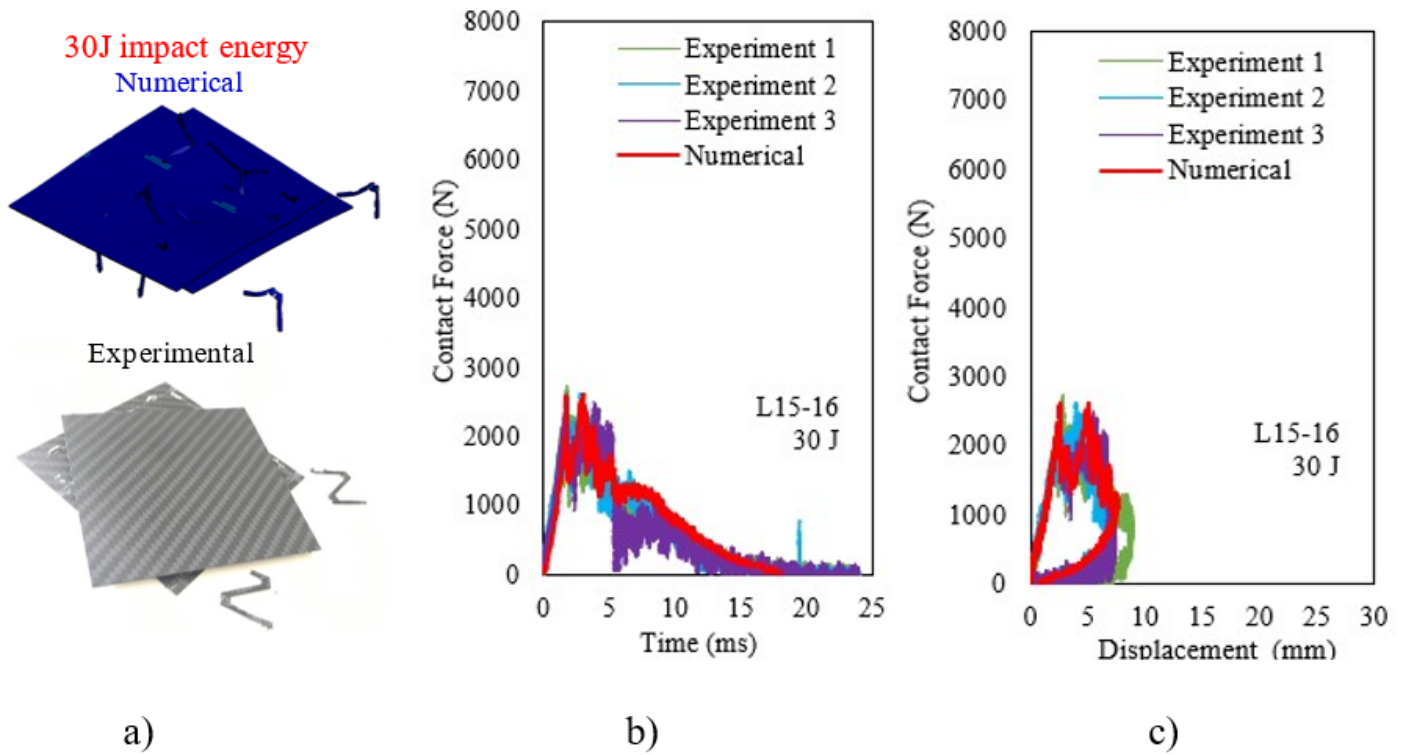
Figure 8

a) Damage behavior at 30 J, b) contact force-time c) contact force-displacement graph for the L15-16.
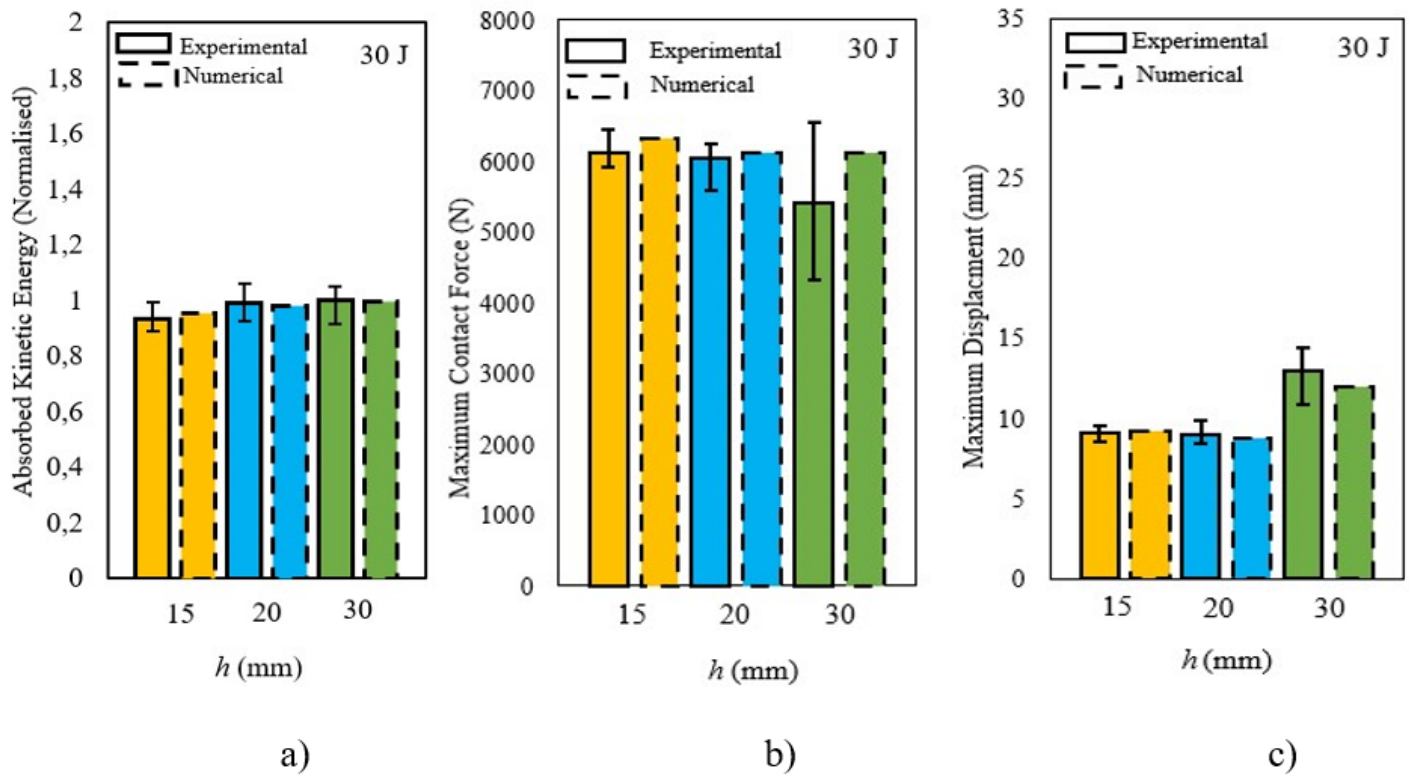
Figure 9

a) Normalized absorbed kinetic energy, b) maximum contact force and c) maximum displacement graph for different cell heights in square core specimens.
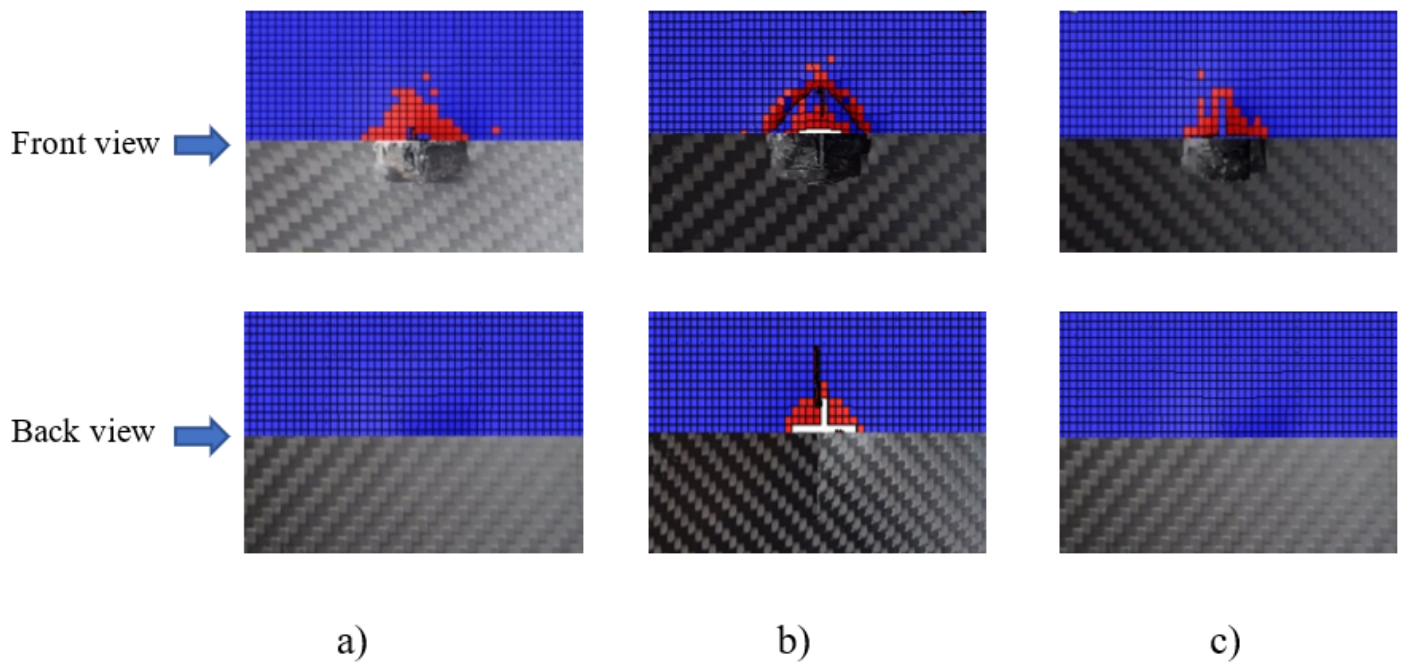
Figure 11

Experimental and numerical comparison of transverse matrix damages for a) S15-16 (30 J), b) E15-16 (30 J) and c) L15-16 (10 J).

a)

b)
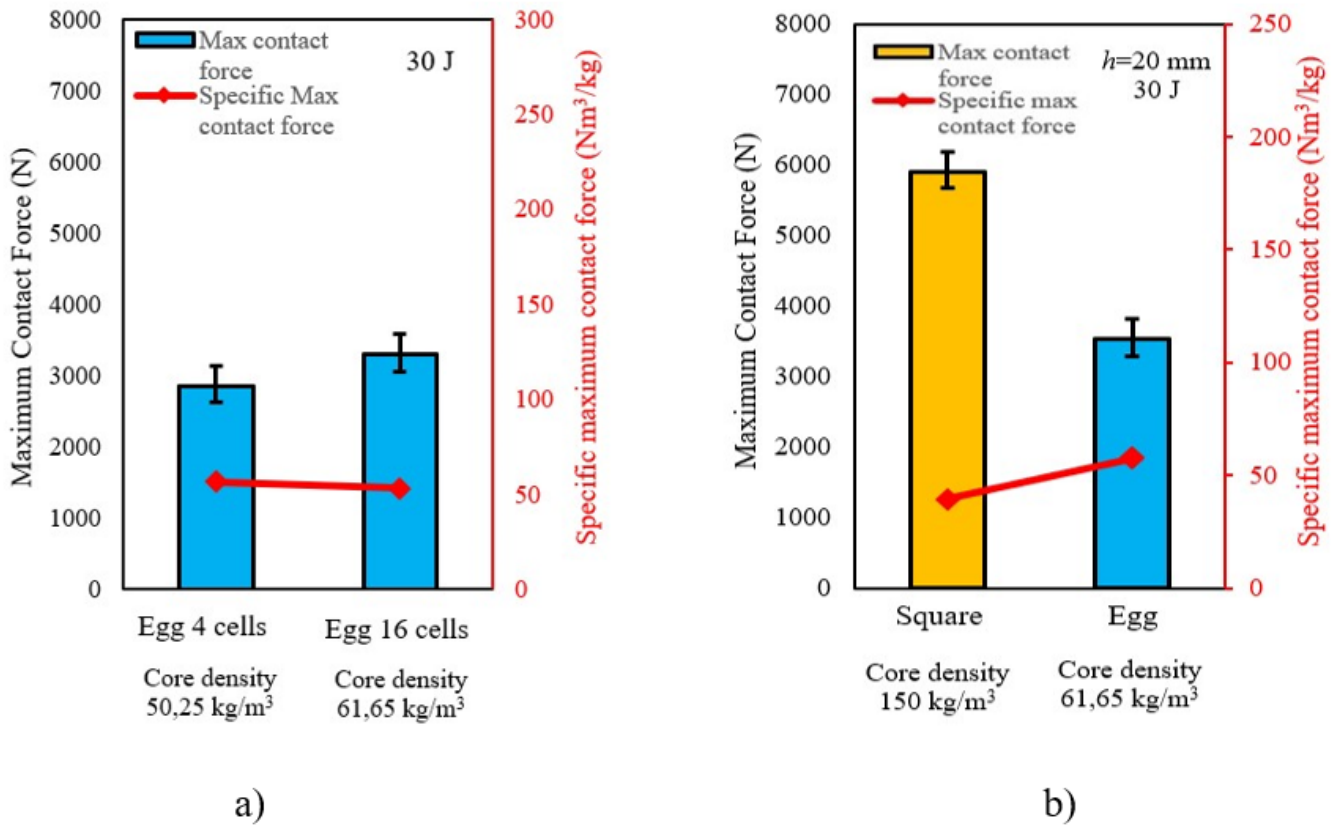
Figure 12

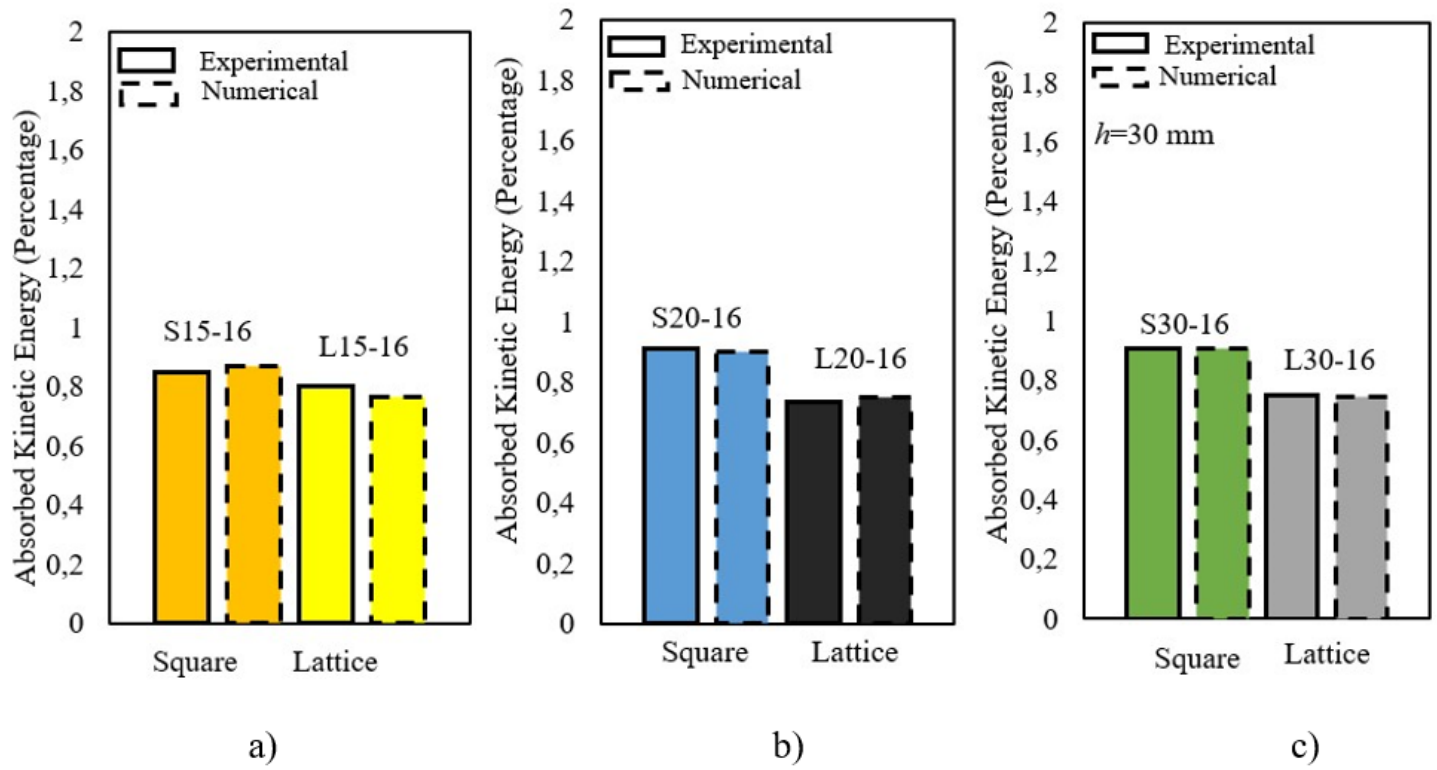Effect of a) cell density for egg core type, b) core type on maximum contact force.

Figure 13

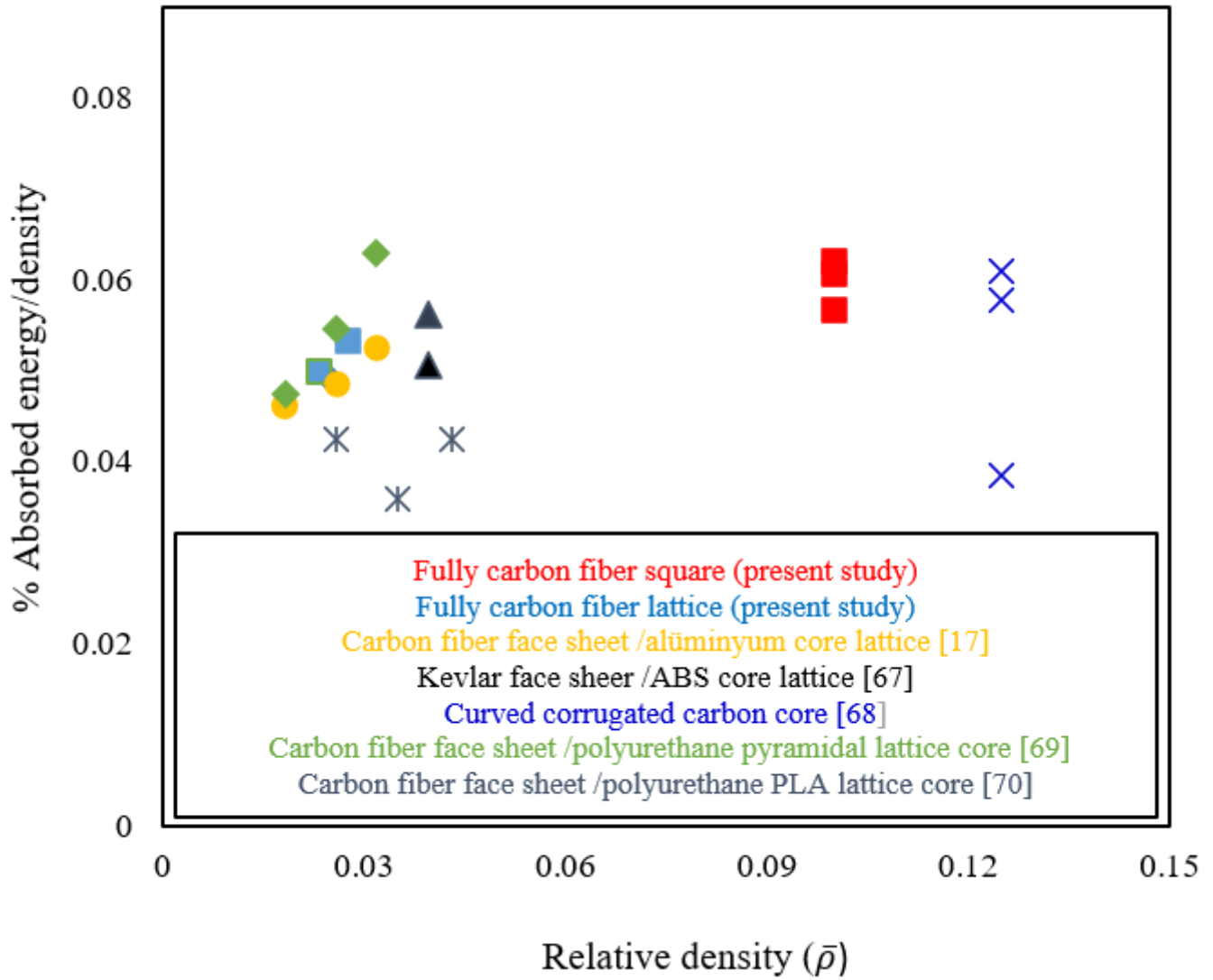Variation of absorb energy with core type for a) h =15, b) 20 and c) 30 mm.

Figure 14

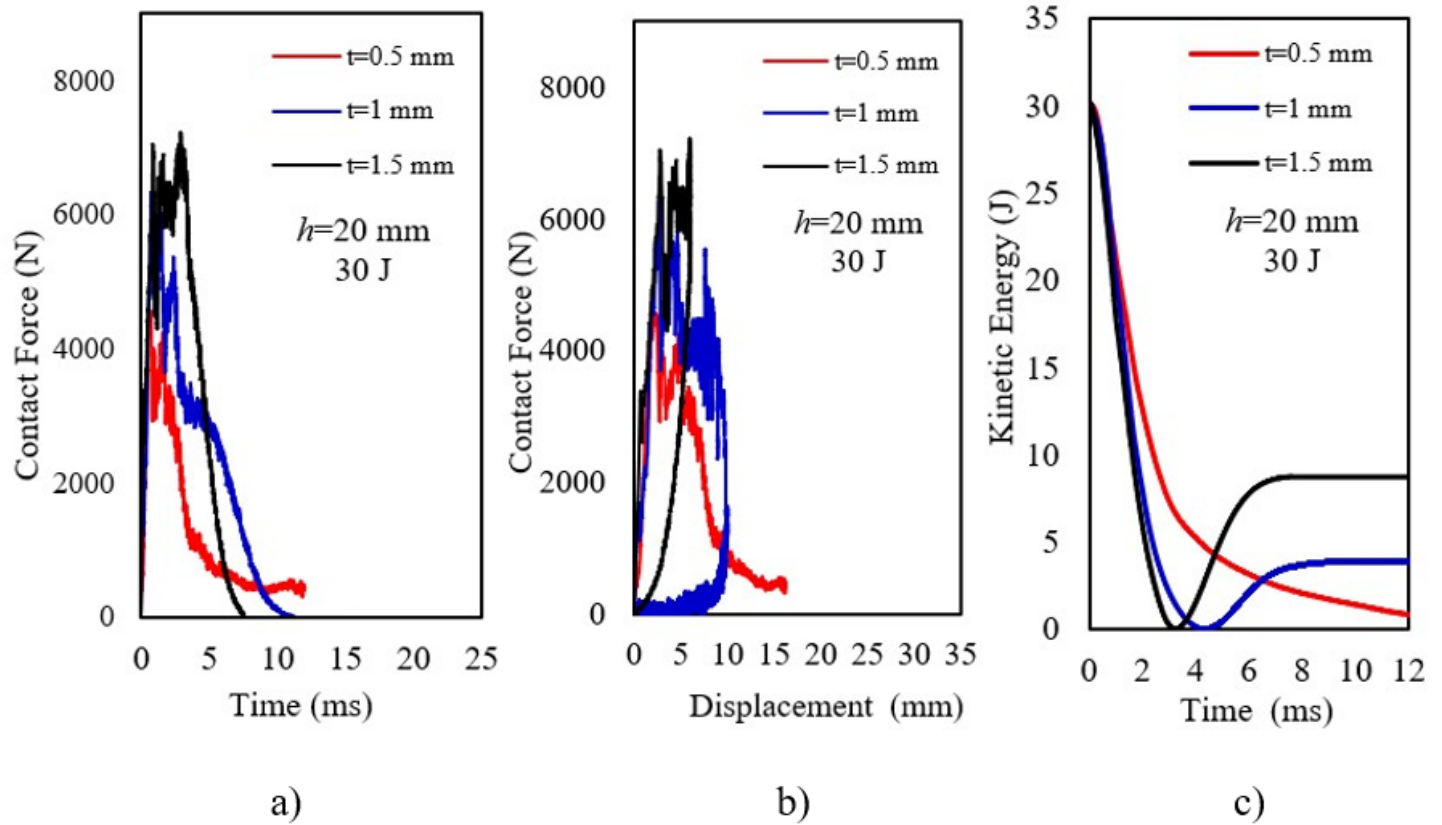Variation of energy absorbed per unit density with relative density.

Figure 15

a) Contact force-time, b) contact force-displacement, c) kinetic energy-time graph of square core sandwich structures with different face sheet thicknesses

Supplementary Files

This is a list of supplementary files associated with this preprint. Click to download.

- Tables.docx